# The cool wake around 4C 34.16 as seen by *XMM-Newton*

I. Sakelliou[1,2], D.M. Acreman[1], M.J. Hardcastle[3], M.R. Merrifield[4], T.J. Ponman[1], I.R. Stevens[1]

[1]*School of Physics & Astronomy, University of Birmingham, Edgbaston, Birmingham B15 2TT*
[2]*Max-Planck-Institute für Astronomie, Königstuhl, 17, D-69117, Heidelberg, Germany*
[3]*School of Physics, Astronomy & Mathematics, University of Hertfordshire, College Lane, Hatfield, Hertfordshire AL10 9AB*
[4]*School of Physics & Astronomy, University of Nottingham, University Park, Nottingham NG7 2RD*

23 June 2007

**ABSTRACT**

We present *XMM-Newton* observations of the wake-radiogalaxy system 4C 34.16, which shows a cool and dense wake trailing behind 4C 34.16's host galaxy. A comparison with numerical simulations is enlightening, as they demonstrate that the wake is produced mainly by ram pressure stripping during the galactic motion though the surrounding cluster. The mass of the wake is a substantial fraction of the mass of an elliptical galaxy's X-ray halo. This observational fact supports a wake formation scenario similar to the one demonstrated numerically by Acreman et al (2003): the host galaxy of 4C 34.16 has fallen into its cluster, and is currently crossing its central regions. A substantial fraction of its X-ray halo has been stripped by ram pressure, and remains behind to form the galaxy wake.

**Key words:** X-rays: galaxies: clusters – X-rays: ISM – ISM: kinematics and dynamics – galaxies: clusters: general – galaxies: interactions

## 1 INTRODUCTION

As a cluster galaxy moves through the intracluster medium (ICM), an X-ray bright region trails behind it, revealing its direction of motion. We now know that there are two physical processes that take place as a galaxy moves through the ICM, and lead to the creation of an overdense wake behind it: i) the accretion of ICM (Bondi-Hoyle accretion; Sakelliou 2000), and ii) ram pressure stripping of the galactic material (Stevens et al. 1999). Naturally, both processes should take place at the same time (e.g., Acreman et al. 2003).

Depending on the properties of the galaxy and the cluster [e.g., the galaxy velocity ($v_{\mathrm{gal}}$) and the temperature of the ICM ($T_{\mathrm{ICM}}$)], wakes behind galaxies may be visible at X-ray wavelengths. An understanding and knowledge of their production mechanisms, of the most favourable conditions for detectable wake production, and of their properties would be very rewarding for two main reasons. Firstly, wakes provide the only general means of finding the direction of the motion of the galaxy in the plane of the sky, thus contributing to the study of the dynamics of clusters (Merrifield 1998). This method of studying clusters has been demonstrated already using both *ROSAT* (Drake et al. 2000) and *Chandra* data (Acreman et al. 2005). Secondly, wakes are manifestations of the galaxy/ICM interactions, which modify the properties of both the cluster (e.g., by contributing to the metal enrichment of the ICM) and the galaxy (e.g., by inducing star formation). Thus, they may provide clues to the transformation and subsequent evolution of galaxies in clusters.

Our aim was to find the X-ray properties of wakes that had been known from the epoch of *ROSAT* . Figure 1 shows the *XMM-*

*Newton* image of a first example: the wake associated with the radio galaxy 4C 34.16. Unfortunately, not many candidates were known from *ROSAT* observations, and we did not have accurate measurements of their properties. *ROSAT* images and spectra of a few systems (M86, Rangarajan et al. 1995; 4C 34.16, Sakelliou et al. 1996; NGC4472, Irwin & Sarazin 1996; NGC1404, Jones et al. 1997) gave the first clues that wakes exist, and that they might be cooler than the surrounding medium. The new instrumentation on *Chandra* and *XMM-Newton* has provided us with some more evidence that wakes might be a common phenomenon: in deep X-ray images of clusters' cores wake-like features have been seen (e.g., Abell 1795 Fabian et al. 2001; Abell 133 Fujita et al. 2002; Abell 2199 Johnstone et al. 2002). Temperature maps of limited resolution also suggest that these filaments are cooler than their surrounding media. As other authors have also argued (e.g., Fabian et al. 2001), wakes must be due to the motion of the central cluster galaxy relative to the ICM. The recent work on the *XMM-Newton* data of M86 has been very instructive, as it has showed that the 'plume' associated with that galaxy is metal rich (Finoguenov et al. 2004). However, in all these cases there has been no independent evidence (at other wavelengths, for example) which could confirm that the galaxy is moving in the direction indicated by the wake.

Confirmation of the direction of motion of 4C 34.16 comes from the shape of its radio jets. 4C 34.16 is a radio source associated with the central galaxy in the cluster Z0357.9+9432. Its plumes are symmetrically bent into a wide C-shape (see Fig. 1). The most widely favoured model invokes ram pressure as the main
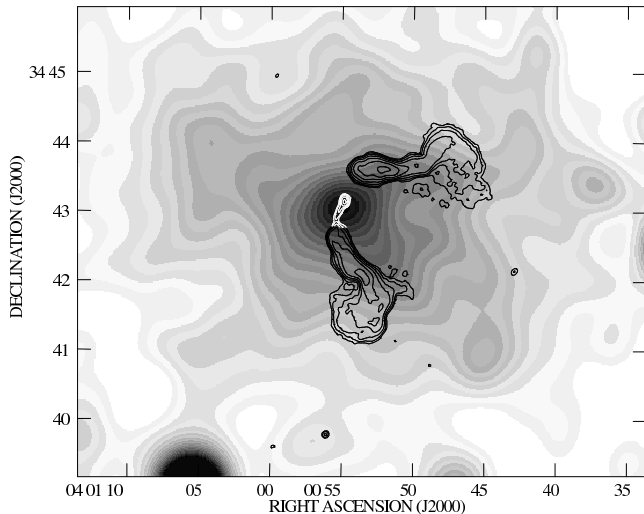
**Figure 1.** *XMM-Newton* and radio data of the field around the radio galaxy 4C 34.16. *XMM-Newton* images from the three imaging detectors (MOS1, MOS2, and PN) in the (0.3-5.0) keV energy range have been co-added, and the mosaic adaptively smoothed. Contours of the radio emission at 1.4 GHz are overlaid.

force responsible for the plume bending. Fortunately, the direction indicated by the bent plumes coincides with the direction of the wake, supporting the models of wake production discussed above.

In this paper we present *XMM-Newton* observations (Section 2) of the field around 4C 34.16. Using these data we derive the properties of the cluster in Section 3, and of the wake in Section 4. Finally, in Section 5 we discuss the most favourable models for the wake production, and find the parameters that are consistent with the observations.

Throughout this paper we use a redshift for 4C 34.16 of 0.078 [NASA/IPEC Extragalactic Database (NED)]. We adopt a Hubble constant of $H_0 = 71$ km s$^{-1}$ Mpc$^{-1}$, and $\Omega_M = 0.27$, which places the source at 349.3 Mpc, and gives a scale of 1.457 kpc arcsec$^{-1}$.

## 2    OBSERVATIONS AND DATA REDUCTION

The field around 4C 34.16 was observed with *XMM-Newton* for $\sim$27 ksec. During the observation the two MOS and PN instruments were operating in the PrimeFullWindow and PrimeFullWindowExtended mode respectively; the medium filter was used for all three instruments. The Optical Monitor (OM) was not switched on, due to the presence of bright stars within the field of view.

The raw event lists from the EPIC instruments were processed and calibrated with SAS v5.3. During the processing the parameter *withbadpixfind* was switched on so that bad pixels that had not been recorded in the calibration files were found and subsequently removed. After the initial processing we confirmed that new bad pixels were found. The calibrated events were filtered for flags, using the *XMM-Newton* flags #XMMEA_EM and #XMMEA_EP for the two MOS and the PN detectors respectively. Restrictions on the pattern were also applied: we kept only events with PATTERN<12 for the MOS cameras, and < 4 for the PN.

The observation was contaminated by background flares, which were apparent in all energy bands. To clean the event lists for image analysis (Section 3.1), the prescription in Read & Pon-

man (2003) was followed. This cleaning procedure left a useful exposure of $\sim$21 ksec for each the two MOS cameras, and $\sim$13 ksec for the PN camera. For the spectral analysis we imposed more strict limits, which reduced the exposures further by $\sim$5 ksec (see Section 3.2).

Using the filtered and clean event files of each imaging *XMM-Newton* instrument, images and exposure maps were created in the (0.3-5.0) keV energy range. The images from all three instruments were finally merged after being exposure corrected, using the SAS task EMOSAIC. Subsequently, the mosaic was smoothed with an adaptive kernel using CIAO's CSMOOTH tool. Figure 1 presents the merged image, with the contours of a 1.4-GHz radio map overlaid.

The radio data consist of 1.4-GHz observations in the B and C configurations of the NRAO Very Large Array (VLA). The B-configuration data were taken by us on 2002 Aug 23; the C-configuration data were obtained from the VLA data archive (programme AM79). Both datasets were calibrated, merged and imaged within AIPS in the standard manner. As previously explained, the central cluster galaxy hosts the double, bent radio source 4C 34.16. In Fig. 2 we show the contour plot of the merged (0.3-5.0) keV image, overlaid onto the DSS optical image of the field around the central galaxy in the cluster, which is the host of 4C 34.16.

It is apparent from Fig. 1 and Fig. 2 that the cluster is fairly spherically symmetric on large scales. The core of the radio galaxy coincides with the peak of the X-ray emission, which is not located at the centre of the inner X-ray emission, but is offset to the northeast. The X-ray emission around the radio galaxy is elongated along a line that bisects the angle between the two radio lobes. As mentioned before, the shape of the radio galaxy indicates a galactic motion to the North-East. Thus, the asymmetrical X-ray emission could be due to a wake trailing behind the galaxy.

In the following sections we use the *XMM-Newton* data to derive the properties of the cluster (Section 3) and the wake (Section 4).

## 3    AVERAGE CLUSTER PROPERTIES

### 3.1    Image Analysis

For the purposes of the following spatial analysis, we generated background subtracted and exposure corrected images independently for each imaging instrument on *XMM-Newton* . Firstly, images for all three instruments were created in the (0.2-4.5) keV energy range. Following Read & Ponman (2003), particle and instrument background maps were created. They were then subtracted from the data images, after scaling them to the out-of-field events. The resulting images were corrected for vignetting by multiplying them by the appropriate vignetting maps.

Our final aim was to compare the properties of the wake with those of its environment, so that we can assess the wake production processes. Thus, we used the above generated data images to derive the spatial properties of the cluster. As Fig. 1, and 2 demonstrate, the X-ray emission from the wake and the galaxy dominate in the inner cluster region, around the active core. At large distances the cluster appears fairly symmetric. In order to derive the average cluster properties and compare them with past results, we fitted the (0.2-4.5) keV particle-subtracted vignetting-corrected images in SHERPA with a 2-dimensional $\beta$-model. Bright point sources were removed, by excluding circular regions around them. We also decided to exclude the inner $\sim$1.3 arcmin around the radio core, and we did not model the emission of the X-ray halo and active nucleus
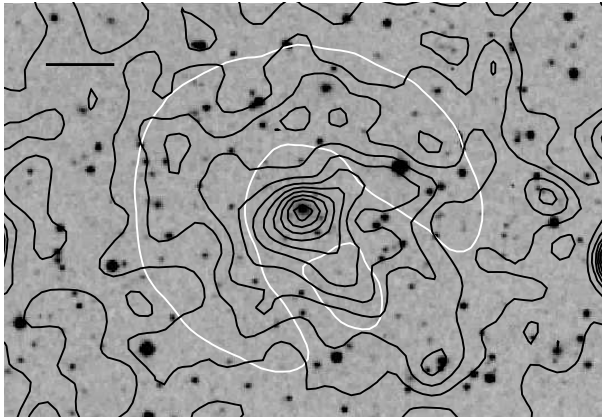
**Figure 2.** X-ray contours of the adaptively smoothed (0.3-5.0keV) mosaic overlaid onto the DSS image around 4C 34.16. The contour levels are linearly spaced from $(1-5)\times10^{-5}$ cnt s$^{-1}$ pix$^{-2}$. The white contours mark the boundaries of the source and background regions that are used for the spectral analysis of Section 4.1. The horizontal bar at the top left corner of the image is 1 arcmin long.

**Table 1.** Properties of the ICM and the Wake

|  | ICM | WAKE |
|---|---|---|
| $N_{\mathrm{H}}$ ($\times10^{22}$ cm$^{-2}$) | 0.172[0.143-0.202] | 0.689[0.288 - 1.280] |
| $T$ (keV) | 3.17[2.66-3.70] | 1.14[0.39-1.94] |
| $Z$ (Z$_{\odot}$) | 0.25[0.09-0.45] | 0.25$^f$ |
| $\chi^2/d.o.f$ | 342.1/260 | 59.8/60 |
| $n$ ($\times10^{-3}$ cm$^{-3}$) | 1.33[1.02-1.64] | 2.37[1.66-8.57] |

NOTES: All the limits reported are at the 90 per cent level, with $\Delta\chi^2 = 2.71$. The abundance table is from Anders & Grevesse (1989), as implemented in XSPEC.
$^f$: the parameter is frozen during the fitting procedure.

during this fitting procedure. The 2-dimensional model was convolved with the appropriate point-spread function (PSF) for each instrument, which is a 2-dimensional image of the PSF of each instrument, as implemented in the SAS task CALVIEW.

Data from the three EPIC instruments were not co-added, but fitted simultaneously. During the fitting procedure, the core radius ($r_c$) and $\beta$ parameter, of the $\beta$-model were linked and left free to vary; the ellipticity was set to zero; and the centre of the distribution was fixed to the location of the active core. The model normalizations were allowed to vary independently for each instrument. This fitting procedure resulted in a best-fitting value for the core radius of $r_c$ =2.371[2.336-2.412] arcmin =207.26[204.23-210.89] kpc, and a $\beta$=0.858[0.829-0.890] ($1\sigma$ limits are quoted), consistent with the *ROSAT* results (Sakelliou et al. 1996). If the centre of the $\beta$-model is left free to vary, the resulting parameters are consistent within the errors with the ones we present above.

Although a derivation of the small scale galaxy's X-ray properties (galactic X-ray halo and active nucleus) is outside the scope of this paper, we attempted to model them. We added another $\beta$-model to describe the galactic halo, and a delta function for the active core. Again, the composite models were convolved with the appropriate instrument PSFs. All trials reproduced the cluster properties found before. However, the galaxy parameters were poorly constrained. Better quality data are required to allow a determination of the galaxy properties.

## 3.2 Spectral Analysis

As mentioned in Section 2, for the purpose of spectral analysis the original event lists were cleaned further leaving useful exposures of ~15.9, ~16.0, and ~10.2 ksec for the MOS1, MOS2, and PN respectively.

To obtain a spectrum of the ICM, we accumulated counts in a circular region centred on the central galaxy and extending out to 5 arcmin. The background spectrum was taken from the same observation, in an annulus adjacent to the source region, and extending from 5 to 8.3 arcmin. Point-source regions were removed from the source and background regions. The emission from the host galaxy of 4C 34.16 and the wake were also excluded from the source re-

gion. Here, as in any subsequent spectral analysis, responses (rmfs) and auxiliary response files (arfs) were generated with RMFGEN-1.48.5 and ARFGEN-1.54.7 respectively.

The spectrum in the (0.3-8.0) keV energy range was modelled in XSPEC by a *mekal* thermal model modified by the line-of-sight hydrogen column, as described by the XSPEC WABS model. The Galactic column in the direction of 4C 34.16 is $N_{\mathrm{H,G}} = 0.162 \times 10^{22}$ cm$^{-2}$. The hydrogen column density ($N_{\mathrm{H}}$), temperature of the ICM ($T_{\mathrm{ICM}}$), metal abundances ($Z$), and normalization were left as free parameters. The results of the spectral analysis of the cluster are tabulated in Table 1, along with the spectral properties of the wake (these will be derived in Section 4.1).

Here it should be noted that the $kT_{\mathrm{ICM}}$ adopted by Sakelliou et al. (1996) was 1 keV. Their temperature was based on relatively poor spectral fits to the *ROSAT* PSPC data. However, in their analysis and interpretation they demonstrated how a larger $kT_{\mathrm{ICM}}$ would have changed the final conclusions. In the following sections it will be apparent how a more accurate measurement of the cluster temperature affects the final results.

In the same table (Table 1) we present the number densities ($n$) of both the cluster and the wake. The tabulated value for the ICM's density is the central number density ($n_0$), derived from the central surface brightness applying eq. (4) from Sakelliou et al. (1996). We calculated $n_0$ for each EPIC instrument independently using the best fit values of the normalizations of the three $\beta$-models found in Section 3.1. The value presented in Table 1 is the weighted mean and error of these three values.

## 4 THE WAKE

Galactic wakes appear as excesses of X-ray emission in the images of galaxies in clusters. Such an enhancement is seen in the (0.3-5.0) keV image of 4C 34.16 (see Fig. 2).

The plot of Fig. 3 clearly shows the asymmetry between the front and behind the galaxy. In this plot we compare the radial profiles taken in regions that lie in front of and behind the galaxy. For the derivation of these profiles we used the background subtracted, (0.2-4.5) keV, mosaic image discussed in Section 3.1. Both profiles were centred on the core of 4C 34.16. Counts were accumulated in concentric annuli of 8 arcsec width. The 'in-front' profile was extracted in a sector between (100-140) degrees, and the 'back' one in a sector between (280-320) degrees, where zero degrees coincides
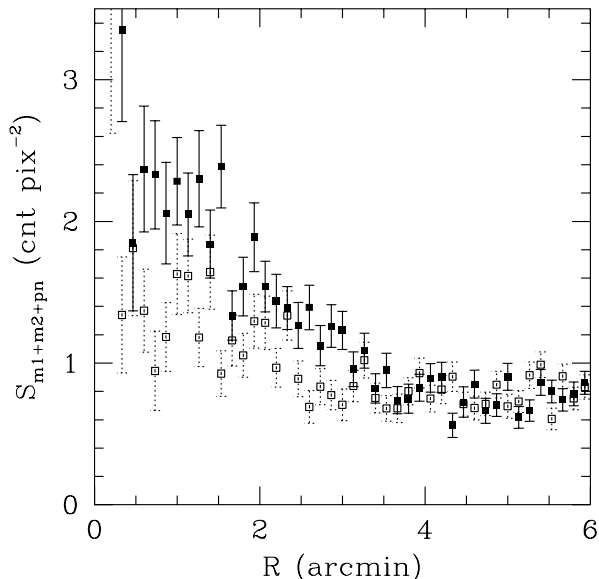
**Figure 3.** Comparison of the radial profiles around 4C 34.16 in two sectors. The 'in-front' profile is shown by open squares, and the 'back' one by filled squares (see Section 4 for details).
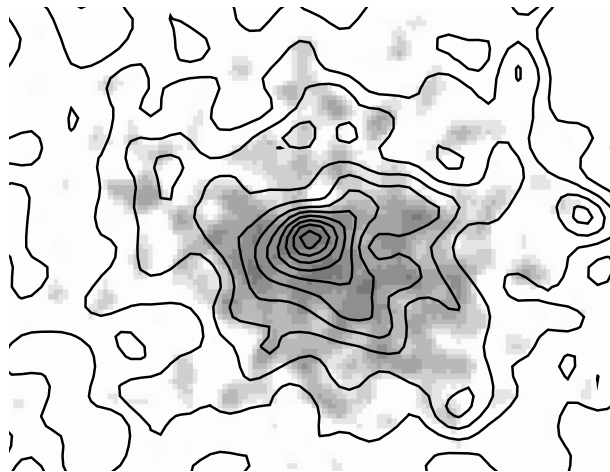


**Figure 4.** X-ray contours of the adaptively smoothed mosaic *XMM-Newton* image in the (0.3-5.0) keV energy range (as in Fig. 2) overlaid onto the softness ratio image (S-H/S+H), where S is the soft band and H the hard band [S=(0.3-1.0) keV and H=(1.0-2.0) keV)]. Darker shades of grey mark regions of softer emission.

with the positive $x$-axis of the image, and angles are measured anti-clockwise. This plot shows clearly that there is an excess of X-ray emission behind the galaxy, and that the disruption extends out to ∼3 arcmin.

Generally, a galactic wake is expected to have softer emission than the surrounding cluster. In order to investigate whether this is true for the 4C34.16 wake, we constructed the softness ratio image shown in Fig. 4. Images for each *XMM-Newton* camera were created from the clean and filtered event lists in the (0.3-1.0) keV, and (1.0-2.0) keV energy ranges. As before, we generated exposure-corrected mosaic images in each energy band, using the SAS task

EMOSAIC. The softness-ratio image of Fig. 4 was calculated by $\frac{S-H}{S+H}$, where $S$ is the softer and $H$ is the harder image respectively. In order to better locate the emission that appears in this image and to guide the eye, we overlay the contours of the (0.3-5.0) keV mosaic, presented in Fig. 2. It is apparent that the softest regions are dominated by emission from the wake.

Thus, the above discussion shows that there is enhanced X-ray emission from the region behind the galaxy, and that this emission is softer than the surrounding cluster.

### 4.1  Wake's spectrum

Driven by the above results, we used the spectra of the wake to derive its temperature and number density, to assist the investigations of the wake production mechanisms that we will carry out later in this paper.

In order to obtain the spectrum of the wake we followed the steps set out in Section 3.2. The source and background regions that were used are shown in Fig. 2. The background region was chosen so that the emission from the cluster at the same off-source radius as the wake region is subtracted, while avoiding regions close to the wake that might be contaminated by wake emission.

The source spectrum was fitted in XSPEC by an absorbed *mekal* model, in a similar manner as done for the cluster in Section 3.2. The hydrogen column ($N_{\mathrm{H,w}}$), temperature ($kT$), and normalization ($norm$) were left as free parameters. The metal abundances ($Z$) were held fixed to the value found for the surrounding ICM ($Z$=0.25 $Z_\odot$, Table 1). Given that we argue later in this paper that the wake consists mainly of galactic material we fixed the metal abundances to the higher value of $Z$=1 $Z_\odot$, and performed the same fitting procedure. We obtained a sighly higher temperature for the wake than the one found for $Z$=0.25 $Z_\odot$ (see Table 1) of $1.44[1.02 - 2.19]$ keV. However, since there is not a well established value for the metal abundance of central cluster galaxies, and since the data do not allow us to measure it directly, we have no reason to adopt a higher value for $Z$.

The spectral fit for the wake resulted in a normalization for the *mekal* component of $norm = 0.6[0.3 - 8.0] \times 10^{-18}$ cm$^{-5}$. Using the dependency of $norm$ on the density ($n$) ($norm \propto \int n^2 \, dV$), we derived a density for the plasma in the wake ($n_{\mathrm{w}}$) of $2.37[1.66 - 8.57] \times 10^{-3}$ cm$^{-3}$. The volume of the wake ($V_{\mathrm{w}} = 1.6 \times 10^{70}$ cm$^3$) was calculated from the dimensions of the wake's region shown in Fig. 2, assuming cylindrical symmetry (i.e., the wake is as extended along the line-of-sight as on the plane of the sky), and that it is on the plane of the sky. For the calculation of the wake's density, we further assumed that the hot X-ray emitting component at the derived temperature is distributed uniformly in the entire volume of the wake.

However, the numerical simulations (Stevens et al. 1999; Acreman et al. 2003) show that the average volume filling factor ($f$) for the material that is at a temperature of ∼1 keV is between 0.3 and 0.4. For a given X-ray luminosity from a given volume, the inferred density scales as $n_{\mathrm{w}} \propto f^{-0.5}$. Thus, it can be larger than the calculated value of Table 1. For a filling factor of 0.35, for example, the density of the non-uniformly distributed wake material is 1.7 times larger than the tabulated value, bringing it up to $4.03[2.82 - 14.57] \times 10^{-3}$ cm$^{-3}$. Both values are consistent within the errors. In the following sections we use the wake density given in Table 1, and a volume filling factor of $f = 1$, and we discuss, when necessary, the implications for $f < 1$.

The wake's properties derived from the above spectral modelling are presented in Table 1. The comparison of $N_{\mathrm{H,w}}$ with that

found from the cluster fits and the $N_{\rm H,G}$ indicates the presence of some extra absorbing material ($N_{\rm H,w} - N_{\rm H,G} = 5.27[1.26 - 11.18] \times 10^{21}$ cm$^{-2}$) associated with the wake. This excess of absorption towards the central parts of the the Z0357.9+9432 was noted before in the *ROSAT* data, and now with *XMM-Newton* we know that it is restricted to the wake region. However, lacking the appropriate data (e.g., HI 21cm radio maps) we cannot be confident that it is due to the presence of neutral material in the wake. This neutral material could be stripped from the galaxy, and cause the absorption of the X-rays towards the wake.

## 5 DISCUSSION

### 5.1 The bent radio galaxy 4C 34.16

4C 34.16 is a wide-angle tailed (WAT) radio galaxy, and therefore shows an abrupt 'flaring' in its radio jets (Hardcastle & Sakelliou 2004, Jetha et al. 2005, Hardcastle, Sakelliou & Worrall 2005). The jets in these sources stop suddenly at some tens of kpc from the radio core. After their termination point, large plumes emerge that are thought to be shaped by the interactions with the surrounding medium.

The jets in 4C 34.16 are transformed to plumes at ~50 kpc from the radio core. These plumes are bent symmetrically into a C-shape (see Fig. 1). The main force acting on the plumes seems likely to be the ram pressure resulting from the motion of the galaxy relative to the ICM. The same motion should be responsible for the creation of the wake, as the wake direction coincides with the direction in which the plumes are bent. Buoyancy makes an additional contribution, dragging the plumes towards the outskirts of the cluster. After the termination point, the plumes can be traced out to a drojected distance of ~(120-140) kpc.

By considering the balance of buoyancy and ram pressure forces Sakelliou et al. (1996) used the *ROSAT* data to set an upper limit on the galaxy velocity of $v_{\rm gal} < 300$ km s$^{-1}$. With the new parameters derived from the *XMM-Newton* observations [$kT_{\rm ICM} = 3.17$ keV compared to 1 keV used by Sakelliou et al. (1996)] the allowed limits allowed by eq. (12) of Sakelliou et al. (1996) are somewhat higher. Depending on the exact orientation and geometry of the flow inside the plumes, the required $v_{\rm gal}$ would be $\sim 1000$ km s$^{-1}$ if the plumes are light compared to the surrounding medium. The projected length of the plumes, on the other hand, sets a lower limit of $v_{\rm gal} > 1200$ km s$^{-1}$ if we think that the plumes are just passive clouds left behind by the motion of the galaxy. But we have independent reasons to believe that the plume physics is more complicated, and we cannot make accurate estimates of the galaxy speed from the radio galaxy structure alone because we cannot measure the particle density or fluid flow speeds in the plumes directly.

Taking into account the above discussion about $v_{\rm gal}$, in the next section, we assess the wake production mechanisms demonstrating the implications of a galaxy speed $> 1200$ km s$^{-1}$.

### 5.2 Wake production

As mentioned in the introduction, two physical processes can produce galactic wakes: Bondi-Hoyle accretion and ram pressure stripping. Of course, both processes take place simultaneously (e.g., Acreman et al. 2003). However, Bondi-Hoyle accretion generates pronounced wakes when the galaxy velocity is sub- or transsonic, and its length does not exceed a few kpc. For exam-

ple, in a 3-keV cluster a Bondi-Hoyle wake cannot be longer than ~5 kpc (Sakelliou 2000). Additionally, the accretion radius [$R_{\rm acc} = 2\,G\,M_{\rm gal}\,/\,(v_{\rm gal}^2 + c_s^2)$] is smaller in richer clusters; in a 3-keV cluster, $R_{\rm acc}$ is ~13 kpc if the galaxy is moving at the sound speed, and it reaches only ~19 kpc if $v_{\rm gal} \simeq 0.6c_s$. Thus, in 4C 34.16 Bondi-Hoyle accretion can only supply the galaxy with ICM material, increasing the mass of its ISM. The mass accretion rate ($\dot{M}_{\rm acc,BH}$) should depend on the galaxy and cluster properties as $\dot{M}_{\rm acc,BH} \propto \pi\,R_{\rm acc}^2\,n_{\rm ICM}\,v_{\rm gal}$. Using a $v_{\rm gal} = 890$ km s$^{-1}$ equal to the local sound speed ($c_s$), $n_{\rm ICM} = 1.33 \times 10^{-3}$ cm$^{-3}$ (Table 1), and $R_{\rm acc} \sim 13$ kpc (Sakelliou 2000), we find that the rate at which ICM is accreted onto the galaxy is $\dot{M}_{\rm acc,BH} \simeq 10\,{\rm M}_\odot$ yr$^{-1}$. It will be apparent that such accretion rates are small compared to the mass of the wake that has already been accumulated.

On the other hand, ram-pressure stripping dominates in the supersonic regime. Taking into account the discussion of Section 5.1 we can deduce that the most possible production mechanism for the wake in 4C 34.16 is ram pressure stripping. Of course, some small contribution (indirectly) from the ICM into the wake's body is also expected, but it should not be substantial compared to the stripped material.

### 5.2.1 The mass of the wake

In Section 4.1 we measured the density of the wake (Table 1). Multiplying the density of the wake $n_{\rm w}$ by its volume $V_{\rm w}$, we find a mass of $M_{\rm w} = 2.3[1.6 - 8.4] \times 10^{10} M_\odot$, which is comparable to the masses of the X-ray halos in elliptical galaxies (e.g., Canizares, Fabbiano & Trinchieri 1987). The material with $M_{\rm w}$ is contained in a region between 45 and 135 arcsec from the galactic core. As mentioned in Section 4.1, the filling factor of the cool wake material may be smaller than 1. A filling factor of $f = 0.35$ implies that the mass of the wake is $f^{1/2} = 0.59$ times the value calculated above, but it is still within the quoted errors. A filling factor as small as 0.01 would be required to reduce the calculated mass by an order of magnitude, but such a filling factor is unrealistically small.

If we assume that all the mass calculated above ($M_{\rm w} = 2.3[1.6 - 8.4] \times 10^{10} M_\odot$) has been accumulated during the time taken for the galaxy to cross the current length of the wake (~130 kpc), we find that the wake must have been created during the past $1.0 \times 10^8$ yr, where a galaxy velocity of $v_{\rm gal} > 1200$ km s$^{-1}$ (Section 5.1) has been used. To create such a wake over this time period a relatively large mass accretion rate of $\dot{M}_{\rm w} \simeq 200\,{\rm M}_\odot$ yr$^{-1}$ is required. Of course, a volume filling factor of 0.35 would reduce $\dot{M}_{\rm w}$ to approximately half the quoted value, and only a $f = 0.01$ would reduce it by an order of magnitude, which would make it comparable to $\dot{M}_{\rm acc,BH}$ (see Section 5.2). We will return to the issue of this relatively large $\dot{M}_{\rm w}$ in the following sections.

### 5.2.2 Comparison with the simulations

All the previous results and discussion suggest that the most probable origin of the wake is through ram pressure stripping, and that the galactic motion is trans- or mildly super-sonic. Additionally, from Section 5.2 we have a first indication that the mass accretion rate into the wake is substantial, and that the mass of the material that has already accumulated is comparable to the total mass of the X-ray halos in elliptical galaxies.

**Table 2.** Simulations

| (I) | (II) | (III) | (IV) |
|---|---|---|---|
| No | $v_{\rm gal}$ (km s$^{-1}$) | $\alpha_*$ ($\alpha_{*,m}$) | $\dot{M}_{\rm rep}$ ($M_\odot$ yr$^{-1}$) |
| 1 | 1200 | 27 | 92.1 |
| 2 | 1200 | 81 | 276.2 |
| 3 | 5000 | 27 | 92.1 |
| 4 | 5000 | 81 | 276.2 |

NOTES: $\alpha_{*,m}$ is the specific mass loss rate at the present day [$\alpha_{*,m} = 5.4 \times 10^{-20}$ s$^{-1}$ (Mathews 1989)]. The mass $\dot{M}$ is calculated by $\dot{M}_{\rm rep}=\alpha_* \times M_{\rm gal}$ (see 5.2.2 for more details).

To test the above ideas, and to gain a better understanding under what conditions such wakes can be created, we decided to compare the *XMM-Newton* results with hydrodynamical simulations of a galaxy moving through the ICM of a cluster. Similar simulations have been presented elsewhere (Stevens et al. 1999; Acreman et al. 2003). In our simulations, a galaxy with mass of $M_{\rm gal} = 2 \times 10^{12}\ M_\odot$ is set into motion in a cluster of temperature $T_{\rm ICM}$ equal to the value given in Table 1.

We ran a number of simulations varying the galaxy velocity ($v_{\rm gal}$) and specific mass loss ($\alpha_*$). We present here a set of four runs that best show the dependency of the results on the input parameters, and provide the best match to the *XMM-Newton* results. The $v_{\rm gal}$ and $\alpha_*$ used for each run are given in Table 2 in columns (II) and (III) respectively. The specific mass loss $\alpha_*$ is a measure of the mass that is replenished ($\dot{M}_{\rm rep}$) within the galaxy from a combination of stellar mass loss and supernovae (see for more details in Stevens et al. 1999). In Table 2 [column (IV)] we also list the $\dot{M}_{\rm rep}$ used in the different simulation runs, that is calculated by $\dot{M}_{\rm rep}=\alpha_* \times M_{\rm gal}$.

Temperature and density cuts along a line parallel to the direction of the galactic motion are presented in Fig. 5(a) and (b) respectively, using the simulated data from all four runs. In Fig. 5(a) we see that in the low velocity regime the temperature of the wake does not reach the measured value, but is on average >2.2 keV. However, increasing the mass replenishment rate (run 2) results in the appearance of cold tongues of material that emanate episodically from the galaxy. These cold features could bring the temperature of the wake down to the measured values. Increasing the mass replenishment rate means that more cold gas is available within the galaxy to be stripped and added into the wake. However, in simulation 2, the ram pressure is not strong enough to strip the galaxy, and most of the cold gas ends up accumulating around the galactic centre, increasing the density in the galactic core as seen in Fig. 5(b). Higher galaxy velocities are required to make this cold material accrete into the wake [Fig. 5(a)]. As we see in the run 4, the temperature of the wake in the region (320-460) kpc (which is the distance from the radio core where we measure the X-ray properties of the wake of Table 1) drops down to ∼1.5 keV, which is within the range of wake temperatures we measure. In Fig. 5(b) we see that in the same region the wake is overdense by a factor between 1.7 and 3.4, again consistent with the measured ratio from the *XMM-Newton* data (see Table 1).

Thus, a galaxy that is moving at a constant velocity > 1200 km s$^{-1}$ through a medium with a uniform density equal to the central density of the 4C 34.16 cluster, could produce a wake with the measured properties, but *only if $\dot{M}_{\rm rep}$ is as high*

*as* ∼ 300 $M_\odot$ yr$^{-1}$. Such mass replenishment rates are high, especially for a central cluster galaxy which is a radio galaxy. This becomes clearer if one thinks that the mass replenishment rate in the nearby starburst galaxy M82 does not exceed a few tens of $M_\odot$ yr$^{-1}$. Thus, we consider the previously presented scenario unrealistic, as the host galaxy needs to contain a huge amount of cold material, to be stripped by ram pressure and accreted onto the wake.

### 5.2.3 A more realistic scenario

We have found that the mass of the wake is a substantial fraction of the X-ray halo of an elliptical galaxy and large accretion rates are required to produce it. The only alternative to the Section's 5.2.2 scenario for the wake production is that of a galaxy with a pre-existing halo falling into a cluster: a galaxy with a substantial hot interstellar medium (ISM) has fallen into the cluster, and is currently crossing the central region of the cluster; its halo is stripped severely during this crossing, and most of the pre-existing halo forms its wake.

The large-scale structure of the ICM provide support to this picture. The *ROSAT* images (Sakelliou et al. 1996) showed that the ICM at large radii is elongated along a direction coincident with the direction of the wake and the bent jets. This characteristic was attributed to a recent disruption of the cluster by a small in-falling group. Such a process has been demonstrated numerically with the recent simulations of Acreman et al. (2003). They modelled a spherical galaxy that is falling into a cluster not very different from the one around 4C 34.16 (they used a cluster temperature of 2.7 keV, while the ICM of the 4C 34.16 cluster is at ∼3.2 keV (see Section 3.2). Their work showed that: i) the galaxy velocity becomes mildly super-sonic during the core passage (see their fig. 1); ii) most of the halo is stripped during the first core crossing (see fig. 3 and 4 in Acreman et al.); iii) the galaxy can lose half or more of its ISM during its initial travel towards the cluster centre.

According to the above scenario 4C 34.16 should not retain the large quantities of ISM found in similar sources (e.g., Jetha et al. 2005, Hardcastle et al. 2005). In order to see if this is true, we attempted to model the galaxy spectrum in XSPEC. The source region was a circle of 10 arcsec radius around the active core. We fitted the spectrum with a *mekal+power law* model modified by the Galactic absorption. The temperature ($kT_{\rm ISM}$), power law index ($\Gamma$), and normalizations of the two models were left free to vary. This fitting procedure resulted in a $kT_{\rm ISM}$ of 0.2 keV and $\Gamma = 2.3$ ($\chi^2/d.o.f$=15/14). However, the small number of observed counts meant that the best-fitting parameters were not well constrained. We found that the unabsorbed luminosity of the thermal component only in the (0.6-3.5) keV energy range is ∼ 0.3 × 10$^{42}$ erg s$^{-1}$, lower than the luminosity of the ISM in 3C 465 (2 × 10$^{42}$ erg s$^{-1}$, Hardcastle et al. 2005), suggesting that there might be a lack of hot gas from the galaxy in 4C 34.16.

The close match of the Acreman et al. (2003) results and the X-ray properties of the 4C 34.16 supports strongly the idea that the process simulated by Acreman et al. (2003) represents the best explanation in hand for what is happening around 4C 34.16.

### 5.2.4 Is there a compression region in front of the galaxy?

According to the proposed scenario the host galaxy is currently crossing the cluster core and its velocity is mildly supersonic. Such
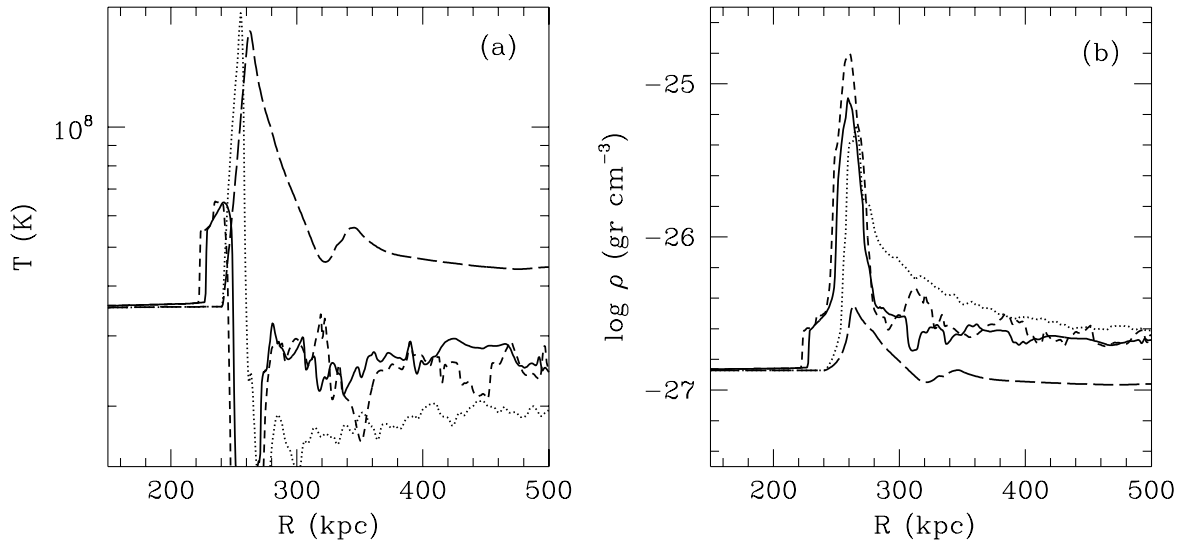
**Figure 5.** Temperature (a) and density (b) variations along a line parallel to the galaxy velocity. Both cuts are derived from the simulated data. The galaxy is moving to the left of the image, and its centre is at ∼260 kpc. Simulation runs No 1, 2, 3, and 4, are represented by a solid, short dashed, long dashed, and dotted lines respectively (see Table 2 for details).
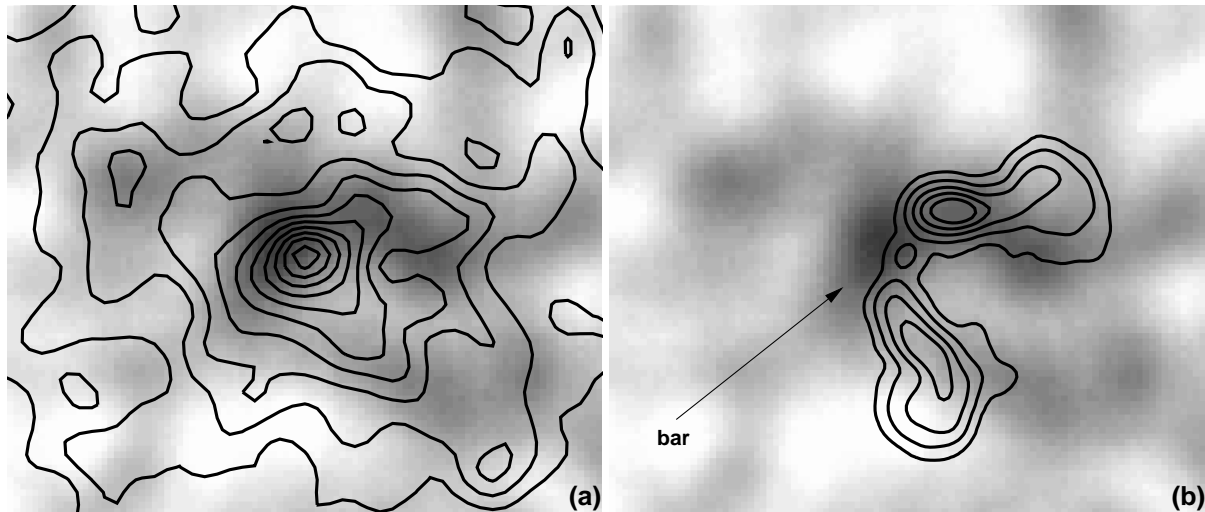


**Figure 6.** (5.0-8.0) keV image overlaid by (a) the (0.3-5.0) keV contours, and (b) the radio map.

a motion should compress the region in front of the galaxy, resulting in the heating of the ICM. The galaxy is moving relative to its surroundings with a Mach number of $M > v_{\rm gal}/c_{\rm s} \sim 1200/890 = 1.35$, the compression factor is $1/x > 1.5$. From Landau & Lifshitz (1987) we find that such a compression would increase the temperature of the medium in front of the moving galaxy from ∼3.17 keV up to $kT_{\rm b} > 5$ keV (in the above calculation we use $\gamma = 5/3$). This effect can been seen clearly in the results of the simulations in Fig. 5(a), where the temperature in front of the galaxy is enhanced.

The presence of such a hot feature in the *XMM-Newton* data would provide further support for a supersonic motion. Figure 6 shows an *XMM-Newton* image in the (5.0-8.0) keV range. Again, this mosaic is produced in a similar manner to the ones of Section 2,

and smoothed with a Gaussian kernel with $\sigma = 20$ arcsec. As can be seen in this image the emission from the wake is not visible, as expected, since we have found its emission to be soft and dominant in the soft energy bands. The hard image reveals a potentially intriguing feature. There appears to be a 'bar' of bright emission in front of the galaxy. This region might be the above-mentioned compression region in front of the galaxy.

The centroid of this 'bar' is ∼18 arcsec away from the galactic centre. One might think that this emission comes from the radio core, but it is very unlike since at other energy ranges there is a very good alignment between the radio core and the X-ray peak. Additionally, we are not aware of pointing errors as large as the measured offset between the 'bar' and the radio core. The 'bar' appears extended and not point-like. It is detected with a S/N∼5

above the local background, which was calculated from the same hard image between 1.5 and 5 arcmin away from the galaxy. The inspection of optical images does not reveal any obvious source that could be responsible for this hard X-ray emission.

To obtain the spectrum of the 'bar', we accumulated counts in an elliptical region in-front of the galaxy with minor and major axes of 12 and 30 arcsec respectively. The background spectrum was taken in an annulus between 1 and 2.5 arcmin, similar to the one shown in Fig. 2 . We fitted the spectrum with an absorbed *mekal* model. The $N_H$ and metal abundance were fixed to the Galactic value and 0.25 respectively. Unfortunately, there are not enough counts in the data to constrain the temperature of the detected feature. The fits indicate that the temperature is $kT_b > 4$ keV ($\chi^2$/d.o.f.=27.3/27). Its unabsorbed luminosity is $L_x[(0.5 - 5.0) \text{ keV}] \simeq 0.7 \times 10^{41}$ erg s$^{-1}$.

Applying the jump conditions from Landau & Lifshitz (1987) for a Mach number of $M > 1.35$, we derived that the density of the 'bar' should be $n_b > 2.0 \times 10^{-3}$ cm$^{-3}$. Using PIMMS, we find that the luminosity of a thermal plasma with $T_b$ and $n_b$ properties derived above in the (0.5-5.0) keV energy range is $> 0.2 \times 10^{41}$ erg s$^{-1}$, consistent with the measured value from the *XMM-Newton* data.

Thus, the properties of the hot feature in front of the galaxy might support the previous arguments that the motion of 4C 34.16 is currently supersonic as it is crossing the cluster core. However, better quality data are required to explore this possibility further.

### 5.3    The fate of the wake

Using the densities and temperatures of the ICM and the wake shown in Table 1 we find that the wake is in pressure imbalance, by $P_w/P_{ICM} \simeq 0.64$ (where $P_w$ and $P_{ICM}$ are the thermal pressures of the wake and and ICM at the location of the wake, respectively). The pressure imbalance within the wake will be eliminated within $t_P \sim R_w/c_s$, where $c_s$ is the local speed of sound, and $R_w$ is the radius of the wake. The size of the overpressured wake, as measured from the X-ray data is ($60 \times 120$) arcsec. Using an average radius of $R_w$=65 kpc, we find that the pressure imbalance will disappear in $t_P \sim 0.7 \times 10^8$ yr, assuming that this region of wake material is left behind in the cluster, and that it is not replenished by neither stripped ISM nor accreted ICM. This time is slightly smaller than the core crossing time ($t_S \sim 2.3 \times 10^8$ yr).

On the other hand, the entropy of the wake is less than the entropy of the surrounding medium : $S_w/S_{ICM} \simeq 0.24$ (where $S_w$ is the entropy of the wake and $S_{ICM}$ the entropy of the ICM at the location of the wake). Here, the entropy is defined as $S = \frac{T}{n^{2/3}}$. Entropy imbalances even out by the transport of material towards regions in the surrounding cluster where the entropies match. Thus, the low entropy wake will tend to go towards lower-entropy regions in the cluster, which are at, or close to, the cluster centre, which in the case of 4C 34.16, coincides with its host galaxy. Therefore, if a cool and dense wake is left behind it will move towards the cluster centre by the buoyancy force:

$$\nabla F_B = (\rho_w - \rho_{ICM}) \, g \qquad (1)$$

where $\rho_w$ and $\rho_{ICM}$ are the densities of the wake and the ICM respectively, and $g$ is the cluster's gravitational acceleration:

$$g = -\frac{kT_{ICM}}{\mu \, m_p} \frac{\nabla \rho_{ICM}}{\rho_{ICM}} \qquad (2)$$

Thus, the wake will be driven by an acceleration of

$$\alpha = \left(1 - \frac{\rho_{ICM}}{\rho_w}\right) g, \qquad (3)$$

where for the calculation of $g$ we used eq. (2), and the properties of the cluster, as derived in earlier sections. The time that it will take for the wake to move to the cluster centre is $t_E^2 = 2r_w/\alpha$, where $r_w$ is the current location of the wake relative to the cluster centre. For $r_w \simeq 1$ arcmin, $t_E = 3.3 \times 10^8$ yr.

The large uncertainties of the density of the wake (see Section 4.1) make the comparison of $t_P$ and $t_E$ difficult. With the current determination of the wake's properties it is unclear whether the pressure imbalance will disappear quickly, leaving the entropy structure almost unaltered.

## 6    SUMMARY AND CONCLUSION

We have presented *XMM-Newton* observations of the X-ray wake that trails behind the WAT radio source 4C 34.16.

Our results can be summarized as follows:

• The wake is cooler and denser than the surrounding ICM: its temperature is $\sim$1.14 keV; for a filling factot of $f$=1 its density is $\sim 2.6 \times 10^{-3}$ cm$^{-3}$, and for a more realistic $f$=0.35 it can be 1.7 times the above value.

• A comparison with hydrodynamical simulations shows that the *XMM-Newton* results fit well with the scenario simulated by Acreman et al. (2003): the host galaxy of 4C 34.16 is falling into its cluster, and currently it is crossing the core region, possibly moving supersonically.

• As the galaxy passes through the cluster, it sweeps up the ICM, forming a hotter and denser region in front of it. There is evidence in the *XMM-Newton* for the presence of such a feature, although better quality data are needed to constrain its properties.

### REFERENCES

Acreman D.M., Stevens, I.R., Ponman T.J., Sakelliou I., 2003, MNRAS, 341, 1333

Acreman D.M., Stevens, I.R., Ponman T.J., Sakelliou I., Merrifield M.R., Pinkney J.C., Ledlow M., 2005, MNRAS, in preparation

Canizares C.R., Fabbiano G., Trinchieri G., 1987, ApJ, 312, 503

Drake N., Merrifield M.R., Sakelliou I., Pinkney J.C., 2000, MNRAS, 314, 768

Fabian A.C., Sanders J.S., Ettori S., Taylor G.B., Allen S.W., Crawford C.S., Iwasawa K., Johnstone R.M., 2001, 2001, MNRAS, L33

Finoguenov A., Pietsch W., Aschenbach B., Miniati F., 2004, A&A, 415, 415

Fujita Y., Sarazin C.L., Kempner J.C., Rudnick L., Slee O.B., Roy A.L., Andernach H., Ehle M., 2002, ApJ., 575, 764

Hardcastle M.J., Sakelliou I., 2004, MNRAS, 349, 560

Hardcastle M.J., Sakelliou I., Worrall D.M., 2005, MNRAS, in press

Irwin J.A., Sarazin C. L., 1996, ApJ 471, 683

Johnstone R.M., Allen S.W., Fabian A.C., Sanders J.S., 2002, MNRAS, 336, 299

Jetha N.N., Sakelliou I., Hardcastle M.J., Ponman T.J., Stevens I.R., 2005, MNRAS, in press

Jones C., Stern C., Forman W., Breen J., David L., Tucker W., Franx M., 1997, ApJ., 482, 143

Kempner J.C., Sarazin C.L., Ricker P.M., 2002, ApJ, 549, 236

Landau L.D., Lifshitz E.M., 1987, Fluid Mechanics (Great Britain: Butterworth-Heinemann)

Mathews W.G., 1989, ApJ, 97, 42

Merrifield M.R., 1998, MNRAS, 294, 347

Rangarajan F.V.N., White D.A., Ebeling H., Fabian A.C., 1995, MNRAS, 277, 1047

Read A.M., Ponman T.J., 2003, A&A, 409, 395

Sakelliou I., 2000, MNRAS, 318, 1164

Sakelliou I., Merrifield M.R., M$^c$Hardy I.M., 1996, MNRAS, 283, 673

Stevens I.R., Acreman D.M., Ponman T.J., 1999, MNRAS, 310, 663